Modulation of Equatorial Pacific Circulation through a 1990's composite El Niño–Southern Oscillation cycle**

BERNADETTE M. SLOYAN
Woods Hole Oceanographic Institution

GREGORY C. JOHNSON AND WILLIAM S. KESSLER
NOAA/Pacific Marine Environmental Laboratory, Seattle, Washington

** Woods Hole Oceanographic Institution Contribution Number 11196 and Pacific Marine Environmental Laboratory Contribution Number 2624

Corresponding author address:

Dr. Bernadette Sloyan, Dept. of Physical Oceanography MS# 21, Woods Hole Oceanographic Institution, Woods Hole, MA 02543 (email: bsloyan@whoi.edu)

ABSTRACT

A 24-month 1990's composite El Niño is produced from 172 contemporaneous CTD/ADCP sections. In agreement with studies of individual El Niño events, the composite shows a South Equatorial current transport decrease, North Equatorial Countercurrent transport increase and a surface intensified Eastward Equatorial current that advects the western Pacific warm pool past 170°W during event onset to the mature phase. Equatorial Undercurrent transport, however, appears in this dataset to be maintained near its seasonal values. This erroneous finding results from a bias in the timing of the ADCP surveys that coincidentally crossed the equator when eastward current pulses briefly return the transport to near-normal values. These are probably the result of Kelvin waves excited by westerly wind anomalies. At these times, however, the hydrographic data captures the low-frequency zonal thermocline adjustment.

During El Niño an increase in the equatorward transport of the northern and southern low latitude western boundary currents is found and across 8°S the interior (basin) pathway is less effective in supplying South Pacific subtropical water to the equator. In the central and western Pacific, changes to the zonal, meridional and diapycnal transports in the surface and upper thermocline layers result in a significant slowdown of the shallow tropical overturning circulation. This study also suggests, that high-frequency EUC transport pulses generated at the mature and decay phases of El Niño may induce convergence in the thermocline layers of the eastern Pacific. This mechanism could be important in reestablishing the normal eastern Pacific stratification prior to the sea-surface cooling that signifies the end of an El Niño event.

1. Introduction

The Tropical-Ocean-Atmosphere/Triangle Trans-Ocean Buoy Network (TAO/TRITON) array that spans the tropical Pacific Ocean provide real-time observations of El Niño–Southern Oscillation (ENSO). The array is maintained with twice-yearly cruises along each of 10 meridional lines instrumented with buoys, between 143°E and 95°W which also provide conductivity-temperature-depth (CTD) and Acoustic Doppler Current Profiler (ADCP) surveys between buoy locations from approximately 8°S to 8-10°N. This study uses 172 CTD and ADCP sections between 143°E and 95°W taken mostly during TAO/TRITON maintenance cruises in the 1990s to investigate the evolution of the tropical Pacific circulation through a 13-step bimonthly composite El Niño cycle.

El Niño events result in a redistribution of mass and heat in the equatorial Pacific Ocean. Westerly wind anomalies over the western and central Pacific relax the usual zonal thermocline slope, with shoaling in the west and deepening in the east. The western Pacific warm pool extends into the central Pacific and warm sea-surface temperatures develop in the eastern Pacific. Observations of individual El Niño events at specific locations across the tropical Pacific have been used to characterize regional characteristics of El Niño (e.g. Delcroix et al. 1992; Johnson et al. 2000; Kessler and McPhaden 1995b; Kessler and Taft 1987; McPhaden 1999; McPhaden and Hayes 1990; McPhaden et al. 1990; Picaut et al. 1996, 2001, 2002; Taft and Kessler 1991; Toole and Borges 1984; Wyrtki 1975, 1985). These previous studies also describe transport changes of the equatorial Pacific zonal current during El Niño. During El Niño both the Equatorial Undercurrent (EUC) and the South Equatorial current (SEC) weaken, while the North Equatorial Countercurrent (NECC) strengthens and eastward surface transport develops on the equator. However, the development of any one El Niño event is unique.

In this study we utilize the TAO/TRITON maintenance hydrographic and ADCP surveys to develop an inverse model of the tropical Pacific Ocean circulation that steps through a 24-month 1990's composite El Niño cycle. This study parallels the earlier work of Rasmusson and Carpenter (1982) who built a description of sea-surface temperature and meteorology

from a composite El Niño, but here we consider the ocean circulation. The paper is structured as follows. The data and inverse techniques are described in Section 2 and the evolution of the zonal currents through the composite El Niño cycle in Section 3. Section 4 details the circulation and anomalies between the onset and mature phases of the El Niño cycle. The implications of the circulation anomalies on the development and demise of the El Niño cycle are discussed in Section 5. Conclusions are given in Section 6.

2. Data and Inverse Model Details

a. Data

The late 1980's and 1990's period for which the composite El Niño cycle was developed included four individual El Niño events, 1986-1987, 1991-1992, 1994-1995 and 1997-1998. In general, the SOI index begins its negative trend at the beginning of the calendar year (February +0), reaches its most negative value in the early months of the following year (February +1) and by the middle of year +1 crosses zero and becomes positive through the final half of that year (Fig. 1). However no two El Niño events have exactly the same SOI structure. The 1986-1987 El Niño was shifted by half a year, relative to other events (McPhaden et al. 1990). The period between 1991 and 1994 was a time of prolonged negative SOI and warm conditions in the tropical Pacific, while the 1997-1998 El Niño was characterized by its sudden onset, demise, and strength (record high sea surface temperature in the eastern Pacific) over the observational record period (McPhaden 1999).

FIG. 1.

Following the fitting procedure of Johnson et al. (2002), a linear function of the SOI (Fig. 1) and an annual harmonic were fit to 172 contemporaneous CTD/ADCP sections to construct a 24-month composite 1990's El Niño cycle consisting of 13 bimonthly meridional temperature, salinity and direct velocity sections at ten different longitudes. The section longitudes are 143°E, 156°E, 165°E, 180°, 170°W, 155°W, 140°W, 125°W, 110°W, and 95°W. The reader is referred to Johnson et al. (2002) for a further description of the data and fitting procedures. Sections between 95°W and the coast of the Americas at 8°S and 8°N, produced from historical CTD and XBT data and similar mapping techniques as those applied by Johnson et al. (2002), close the eastern Pacific northern and southern boundaries.

Previous studies have shown good in-phase agreement between the SOI and the eastward migration of the Pacific warm pool or monthly sea-surface temperature (SST) anomalies in the central Pacific (Picaut et al. 1996; Wang 1995). The bimonthly (i.e. February, April, June, August, October, and December) sections that span the 24-month composite El Niño begin in

December of the year prior to central Pacific warming (year -1), through the warming year (year +0) and finally to peak warming in the eastern Pacific at the beginning of year +1 and return to normal conditions by the middle of year +1. The sections are estimated at day 15 of each given month.

Twenty-five "boxes" were defined with meridional and zonal boundaries chosen to distinguish the equatorial and northern and southern off-equatorial sectors in each meridional band and effectively separate the EUC from the SEC (northern SEC(N) and southern SEC(S) branches) and Subsurface Countercurrents (SCCs) (Fig. 2). Boundaries at 143°E, 156°E, and 165°E reflect and define the complex southern hemisphere western boundary (Fig. 2). The 25 "boxes" were analyzed by inverse methods to provide an estimate of the circulation of the tropical Pacific Ocean during the composite El Niño cycle that is consistent with the temperature, salinity and velocity data.

Following Sloyan et al. (2003), the bimonthly direct velocity sections produced from the Johnson et al. (2002) ADCP maps were extended to 500 m by melding these data with geostrophic velocity estimates from the CTD maps below 250 m. At 8°S and 8°N, thermal wind referenced to 895 m plus an Ekman contribution at the surface provided an initial estimate of the meridional (v) velocity. Finally, we utilized the results of Lagerloef et al. (1999) to estimate geostrophic meridional velocities at $\pm 2^{\circ}$ latitude. The reader is referred to Sloyan et al. (2003) for further details on the application of these procedures.

FIG. 2.

b. Inverse model and a prior constraints

Eleven potential density surfaces between the sea surface and 495 m were chosen to divide the upper ocean into 12 layers (Table 1). Mass (M) and salt(S) were conserved in all layers, while temperature (T) conservation was downweighted in each layer (discussed below). The system of simultaneous equations was solved using the Gauss-Markov technique (Wunsch 1996).

TABLE 1.

The inverse model of Sloyan et al. (2003) was novelly modified to accommodate the

temporal evolution of advection and storage of water masses. The conservation equation for a layer bounded by interface m and $m+1$, including the horizontal and diapycnal property transports, Ekman transport, and storage, has the form:

$$\sum_{j=1}^{N}\left[\Delta x_j \int_{h_m}^{h_{m+1}} \rho c_j (U+b)_j dz \; + (E_j c_j)\right] \qquad (1)$$
$$+(w_c A c)_m - (w_c A c)_{m+1} \;\; = \;\;$$
$$\frac{d}{dt}\left(\sum_{j=1}^{N}\left[\left(\frac{c_j \Delta x_j h_j}{2}\right)_y + \left(\frac{c_j \Delta x_j h_j}{2}\right)_{y+1}\right]\Delta l\right)$$

Here Δx_j is the station spacing at pair j, c_j is the property value per unit mass at this pair. The initial estimate of the velocity U is determined from the CTD, ADCP and XBT data, $E_j c_j$ is the Ekman property transport (added to the upper layer initial meridional geostrophic velocity estimates) at pair j, and the $w_c A c$ terms represent the the property diapycnal transports across the bounding isopycnal layers. The R.H.S of (1) represents the time rate of change in the storage within each region of the model, where h_j and Δl are water layer depth at each station pair and distance between bounding meridional sections (y), respectively. We evaluate $\frac{d}{dt}$ by a centered difference in time. The subsequent system of simultaneous equations is solved for the unknown depth-independent velocity adjustments b_j, and the diapycnal property transfer rate w_c (with $c = M, T, S$) for the m-th interface. A discussion of the uncertainty of the initial estimates of the velocity, diapycnal transfer rate and layer conservation requirements is given below.

The model employed in this study differs from that of Sloyan et al. (2003) in several key aspects. While the temporal storage has been added, the air-sea buoyancy and momentum transformation across outcropping isopycnals are not explicitly incorporated because of the difficulty in generating reliable characterization of monthly heat and freshwater flux climatologies during El Niño. In addition, under normal conditions the Tropical Instability Waves (TIW) are an important component of the eastern and central equatorial Pacific heat balance (Baturin and Niiler 1997; Hansen and Paul 1984; Kessler et al. 1998), while during El Niño the TIW activity decreases and their heat flux to the equatorial Pacific is reduced

(Baturin and Niiler 1997; Vialard et al. 2001). Estimates of TIW heat flux over the composite El Niño are not readily available, therefore we are unable to include an explicit representation of the effect of TIW on the upper ocean heat budget in the inverse model. For these reason the heat conservation requirement for all model layers was relaxed. An a priori mass conservation uncertainty of 3 Sv (1 Sv = 1×10^6 m^3 s^{-1}) per layer and 4 Sv for the upper ocean was chosen, with a heat conservation uncertainty of 1 PW per layer, and salt conservation uncertainty dictated by the layer mean salt anomaly times 3 Sv and upper ocean mean salt anomaly times 4 Sv.

We used the satellite-based monthly 10-meter wind speed data from the Special Sensor Microwave/Imager (SSM/I), which are produced as part of NASA's Pathfinder Program (www.ssmi.com), to calculate meridional Ekman property transports (Table 2) to add to meridional geostrophic velocity estimates. Wind stress (τ) was calculated from the SSM/I wind data between 1987 and 2000 following $\tau = C_D \rho_a U^2 (\mathrm{N\ m^{-2}})$, where $C_D = 1.2 \times 10^{-3}$ is the drag coefficient, $\rho_a = 1.22$ kg m^{-3} is the air density, and U (m s^{-1}) is the 10-meter vector wind. The wind stress data for the bimonthly El Niño sections were produced by fitting an annual harmonic and a linear function of SOI, the same procedure used for the CTD and ADCP maps.

TABLE 2.

ADCP data provide estimates of the absolute zonal velocity to which we assigned an a priori variance of $(6 \times 10^{-2}\,\mathrm{m\,s^{-1}})^2$. This error includes instrumental, navigational processing, and mapping errors. The initial meridional velocities at 2°S and 2°N are estimated from a weighted sum of the equatorial β and mid-latitude f plane geostrophic assumptions (Lagerloef et al. 1999; Sloyan et al. 2003). We assigned meridional velocity a priori variance of $(3 \times 10^{-2}\,\mathrm{m\,s^{-1}})^2$ to these sections. The initial meridional velocity estimates at 8°S and 8°N are the relative (geostrophic and Ekman) velocity. An a priori variance of $(1 \times 10^{-2}\,\mathrm{m\,s^{-1}})^2$ was used at these sections.

Previous studies have inferred significant vertical mixing in the tropical Pacific Ocean which has a strong depth dependence (Bryden and Brady 1985; Johnson et al. 2001; Meinen

et al. 2001; Sloyan et al. 2003; Weisberg and Qiao 2000; Wyrtki 1981). Given the expected depth dependency of diapycnal mixing, we assumed an a priori variance for the diapycnal velocity of $(1 \times 10^{-5}\mathrm{m\,s^{-1}})^2$ for the upper 9 isopycnal surfaces ($\sigma_\theta \leq 26.5$ kg m^{-3}) and $(2 \times 10^{-6}\mathrm{m\,s^{-1}})^2$ for denser, deeper isopycnal layers ($26.7 \leq \sigma_\theta \leq 26.85$ kg m^{-3}).

The solution determined by the inverse model is greatly influenced by uncertainties in the initial estimates of the velocity and diapycnal transport (model variance), and conversation statements (solution variance). The conservation statements are solved within their error by minimizing the deviation of the initial lateral and diapycnal transports within their a priori variance. In the equatorial region the specified variation in depth of the a priori diapycnal transport variance allows diapycnal transports above the core of the EUC to be more active in balancing the conservation equation than diapycnal transport below the undercurrent core. Larger a priori variance of zonal velocities at $\pm 2^\circ$, with respect to $\pm 8^\circ$, reflect the greater uncertainty associated with these velocity estimates. Model solutions run with reasonable perturbations to the a priori variances are the same, within the given error, as those presented here.

3. Variability of zonal current transports during the 1990's composite El Niño

The seasonal variability of the tropical Pacific zonal currents (SEC, EUC, and NECC) have been described using both direct current observations, surface buoy and ship drifts, and dynamic height (e.g. Gouriou and Toole 1993; Hayes et al. 1983; Johnson et al. 2002; Kessler and Taft 1987; Reverdin et al. 1994; Taft and Kessler 1991; Yu and McPhaden 1999). An essential feature of the equatorial Pacific seasonal variability is the westward phase propagation of the zonal current anomalies. In the eastern Pacific, EUC maximum transport occurs in May, while in the western Pacific maximum transport is found in July. On the equator, an annual reversal of the westward surface current is associated with the maximum EUC transport. This occurs during boreal fall when the southeasterly trade winds relax. The SEC also have a westward phase propagation with largest seasonal transport variability found in the SEC(N) (Kessler and Taft 1987). In the central Pacific the SEC(S) reaches its maximum transport between mid-to-late April. The seasonal variability of the SEC(N) is six month out of phase with the NECC. At 165°W, the SCCs show no marked seasonal transport variability (Gouriou and Toole 1993). However, the seasonal variability of the SCCs at other locations has not been documented. TABLE 3.

In this study, the annual cycle (SOI=0) of these zonal currents (Table 3) show seasonal variability similar what has been described by previous studies (Fig. 3). Westward phase propagation is evident for all currents, apart from the SSCC. The SEC(S/N) seasonal cycle is clearly seen: SEC(S) between 156°E and 110°W; and SEC(N) between 95°W to 156°E. The seasonal variability of the SEC(N) is larger than that of the SEC(S). The EEC is only found in the western Pacific reaching a maximum between June and October, no surface eastward transport is seen east of 170°W. The SCCs seasonal variability is most marked in the central Pacific with maximum transport in April and minimum in October. FIG. 3.

In the following section we describe the evolution of the zonal currents through the 1990's composite El Niño and anomalies of these currents from the mean annual cycle. The annual "reversal" of the westward surface transport on the equator and eastward surface

transport synonymous with the advection of the western Pacific warm pool to the central Pacific during an El Niño event are described in the EEC. This is a slightly different definition to that employed by Delcroix et al. (1992).

Following Rasmusson and Carpenter (1982) and subsequent modifications by Wang (1995) and Wang and Weisberg (2000) the 24-month 1990's composite El Niño is decomposed into five stages: (1) onset (December -1 to February +0); (2) development (April +0 to June +0); (3) transition (September +0 to November +0); (4) mature (December +0 - February +1, which is when maximum sea-surface temperature anomalies occur in the eastern Pacific); and (5) decay (April +1 to June +1). These terms will be used when comparing the circulation of the tropical Pacific through the El Niño cycle.

a. SEC

The seasonal cycle of the SEC(S) achieves its maximum at 125°W in October, then propagates westward, reaching 165°E in April of the following year (Fig. 3). While the SEC(S) seasonal strengthening is seen in both years of the composite El Niño cycle (left panel, Fig. 4), the maximum transport between 155°W and 156°E is reduced in year +1 when compared to year +0. This is seen in the SEC(S) anomalous transport (right panel, Fig. 4), with reduced westward transport between 156°E and 170°W during October +0 to April +1. The transport anomalies of the SEC(S) propagate westward from the central Pacific at a phase speed similar to the annual Rossby wave. East of 125°W there is a (slight) anomalous SEC(S) transport increase between August +0 and February +1. FIG. 4.

Similar to the SEC(S), the SEC(N) seasonal transport maximum propagates westward from 95°W (Fig. 4). In the central and eastern Pacific, the SEC(N) returns to near normal strength at the end of year +0. In El Niño year +0, however, the SEC(N) seasonal transport maximum does not propagate westward of 140°W. This results in anomalously low SEC(N) transports in the central and western equatorial Pacific between October +0 and April +1 (right panel, Fig. 4). Anomalously weak SEC(N) transport extends to 125°W between December

+0 and April +1.

The SEC(S/N) westward transport propagation corresponds to the seasonal variability in depth of the 20°C isotherm at 5°S and 5°N (Yu and McPhaden 1999), whose variability is greatest at 5°N. The seasonal variation of the 20°C isotherm can be mostly explained by the annual equatorial forced Rossby wave (Chelton et al. 2003; Kessler and McPhaden 1995a; Yu and McPhaden 1999). The Rossby wave is forced by basin interior winds with little contribution from Kelvin waves reflected at the eastern boundary (Kessler and McPhaden 1995a).

The 1990's composite El Niño weakening of the SEC(N/S) in the western and central Pacific agrees with previous analysis of El Niño events (Delcroix et al. 1992; Johnson et al. 2000; Taft and Kessler 1991). At the peak of El Niño, the SEC transport in the western and central Pacific is reduced by 50-75%. In the far eastern Pacific the SEC(S/N) transports are maintained near their mean seasonal values. Johnson et al. (2000) excluded the eastern Pacific sections in their analysis of the seasonal transport at the onset of the 1997 El Niño (January to June) because El Niño conditions were not evident in those sections at that time. At the peak of El Niño (July-December 1997), as easterly wind were restored across the Pacific, the transports of the SEC (and NECC) were near normal seasonal values. The return of easterly winds in the eastern Pacific during the El Niño transition temporarily re-establishes the westward SEC in that region (Kessler and Taft 1987; Vialard et al. 2001). This may be the cause of the return to near-normal SEC(N) transport in the central and eastern Pacific at the end of year +0. The SEC(N) transport increase between June +1 and October +1 (Fig. 4).

The weakening of the SEC at El Niño mature phase and restrengthening at El Niño demise is a signal of the eastward, then westward, advection during the event. These are associated geostrophically with the changes in the depth of the equatorial thermocline: deep thermocline weakens the SEC, then the post-event shoaling strengthens it.

b. EUC

The EUC seasonal cycle is still apparent throughout the 1990's composite El Niño with maximum transport at 125°W occurring in April-June and minimum in December (left panel, Fig. 4). El Niño slightly modulates the seasonal cycle of the EUC in this representation. There is a small (O(10SV)) reduction in the strength of the EUC in the central equatorial Pacific (170-140°W) between December +0 and April +1, coincident with peak warming in the central and eastern equatorial Pacific (right panel, Fig. 4). In the inverse model, the anomalous EUC transport west of 140°W is due solely to a decrease in the EUC upper thermocline transport. No marked decrease in EUC transport during the composite El Niño is found in the eastern region.

The inverse model's maintenance or only slight reduction of EUC transport through the composite El Niño cycle is at odds with previous observational studies (e.g. Delcroix et al. 1992; Firing et al. 1983; Halpern 1987; Johnson et al. 2000; Kessler and McPhaden 1995a; McPhaden and Hayes 1990; McPhaden et al. 1990). These previous studies show a dramatic reduction and or brief disappearance of the EUC in the central and eastern Pacific during individual El Niño events. As noted, our study produces the 24-month composite 1990's El Niño cycle through a fit of data to an annual harmonic and a linear function of the SOI (Section 2). A comparison of the vertical average (0-250 m) equatorial zonal current anomalies at TAO mooring sites to SOI (Fig. 5) shows that negative SOI is associated with negative zonal current anomalies east of 170°W. [This relationship is especially clear in a 90-day smoothed ADCP time series and the SOI (not shown)]. This result seems to suggest that the simple linear regression to SOI used to construct the 1990's composite El Niño cycle should predict a reduction of EUC transport during the El Niño cycle.

Note, however, that the vertically averaged zonal-current-anomaly weakening occurs over timescales of a few months or less, several times during an El Niño event (Fig. 5). These events do not have a clear timing relative to the SOI. This is consistent with the common observation that westerly wind anomalies during El Niño events have both high and low

frequency components (e.g. Delcroix et al. 1992; Kessler and McPhaden 1995b; McPhaden 1999; McPhaden and Hayes 1990; McPhaden et al. 1990; Toole and Borges 1984). The low-frequency component produces a quasi-equilibrium adjustment of the thermocline slope, which weakens the EUC by relaxing the zonal pressure gradient that drives it. Overlaid on the low-frequency response is a high-frequency component to the strong anomalous westerly wind events. These wind events produce pulses of anomalous eastward current as the Kelvin waves pass each mooring site, 2-3 times during each El Niño event (somewhat smoothed by 15-day smoothing in Fig. 5). Thus, the result of western Pacific wind anomalies is a low-frequency weakening of the EUC modulated by significant short-term variability.

Unfortunately the occupations of the CTD/ADCP surveys used in this study frequently occurred by chance during the high-frequency events that restore the EUC velocity to near-normal strength during El Niño, and thereby missed sampling the weak-EUC periods (Fig. 5). The 1991-92 event at 140°W has a couple of sections during the height of westward current anomalies, but there is also a survey during November 1991 when the SOI was strongly negative and the current anomaly weakly positive. At 110°W, the 1991-92 El Niño was missed completely. Ship sampling during the 1997-98 El Niño missed the large westward current anomalies in the central and eastern Pacific. Therefore, the inverse model's finding of the maintenance of near-normal EUC transport during the composite El Niño is due to a sampling bias in the CTD/ADCP data.

This sampling bias prevents us from using the inverse model results to describe the evolution of the equatorial Pacific circulation through the El Niño cycle. It may, however, allow us to speculate on the fate of these high-frequency transport pulses that restore the EUC to near-normal values while the thermocline in the central and eastern Pacific is depressed relative to normal conditions. This topic is approached in Section 4.

FIG. 5.

c. SCCs

In the western and central Pacific the SCCs show significant transport variability during the 1990's composite El Niño (Fig. 4). In the western Pacific during El Niño there is an anomalous transport increase of the SSCC and a similar sized anomalous transport decrease in the central region (right panel, Fig. 4). West of 170°W positive anomalous NSCC transport is found during El Niño (right panel, Fig. 4). In general, there is a transport increase of both SCC's in the western Pacific and decrease in the central Pacific. In the western and central Pacific sectors a decrease and increase in depth of the 12°C isotherm (σ_θ = 26.5 kg m^{-3}), respectively, is associated with the El Niño SCCs anomalous transports in each sector. Our finding of western Pacific SCCs transport increase during El Niño does not agree with Delcroix et al. (1992), who found that the SCCs were relatively steady during the 1986-1987 event.

d. NECC

Following Taft and Kessler (1991), who show that the southern boundary of the NECC is displaced equatorward from its normal position (4°N) to between 2°-3°N during El Niño, we define the NECC as eastward transport of $\sigma_\theta \leq 25.50$ kg m^{-3} and north of approximately 2.4°N (Table 3). The seasonal NECC has a maximum eastward transport in August in the central Pacific and December in the western Pacific (Fig. 4).

Anomalous eastward NECC transport is seen in the western Pacific between October +0 and February +1 coincident with the El Niño mature stage. As the composite El Niño cycle decays (April +1) the NECC transport minimum propagates westward from 95°W to 165°W. During individual El Niño events the baroclinic NECC transport in the central Pacific generally increases, associated with the deepening of the equatorial thermocline (Kessler and Taft 1987; Taft and Kessler 1991).

e. EEC

In the western and central regions, the EEC is principally found within $\pm 2^{\circ}$ of the equator. The eastward surface transport reaches a maximum in El Niño August +0 and February-April +1 in the western and central Pacific (left panel, Fig. 4). Anomalous eastward transport is associated with the EEC in these regions (right panel, Fig. 4). The EEC transport is interrupted between October +0 and February +1 when the SEC(N) briefly re-establishes itself across the equatorial Pacific.

Previous El Niño studies in the western Pacific find the development of eastward surface transport prior to the surface warming in the central Pacific (Delcroix et al. 1992, 2000; McPhaden et al. 1990; Picaut et al. 1996, 2002). Delcroix et al. (1992) also find a temporary weakening of the eastward surface transport and re-establishment of westerly surface transport during the El Niño transition phase.

Eastward surface transport, between 2°S and the equator, is found in the eastern Pacific between February and June of El Niño year +0 and year +1. The eastward transport is similar in both years and may be part of the annual "reversal" of westward equator surface currents (McPhaden and Hayes 1990) which was not seen in the mean annual cycle (Fig. 3). It is only in El Niño year +1 that the weak eastward surface transport east of 140°W is connected to the larger eastward transport in the western Pacific.

In the eastern Pacific, McPhaden and Hayes (1990), note a stronger than normal reversal of the surface current and weaker SEC during the 1986-1987 El Niño event suggesting that eastward warm water advection plays a role in warming the eastern Pacific. They also note, however, that at this time the thermocline was depressed 20-40 m and that near normal easterly winds maintained upwelling of warmer than normal water.

f. Summary

Transport anomalies of the SEC, NECC and the EEC are connected by being due to the fluctuations in the depth of the equatorial thermocline (Fig. 6) and the resulting changes in the

meridional pressure gradient and geostrophic currents. The NECC transport increases and SEC transport decrease, and vice versa occur at same longitude and time. These transport anomalies are the eastward and then westward advective signatures of an El Niño event.

4. Equatorial Pacific circulation at onset and mature El Niño phases

As shown in Section 3, the timing of hydrographic CTD and ADCP surveys was biased towards sampling the high-frequency El Niño component resulting in periods when the EUC briefly returned to near-normal velocity. The increased EUC transport during these periods occurs when the equatorial thermocline is shallow in the west and deep in the central and eastern Pacific with respect to normal conditions (Fig. 6).

The thickness difference between the composite El Niño onset (February +0) and mature (February +1) phases shows that the water layer lighter than $\sigma_\theta \leq 25.5$ kg m^{-3} shoals in the western Pacific by approximately 10-20 m, and deepens in the central and eastern Pacific by 20-30 m (Fig. 6). The change in thickness of the warm water layer between El Niño October +1 (return to normal conditions with warm water pool confined to western Pacific) and October +0 (warm water pool moving from western to central Pacific) shows that the equatorial Pacific thermocline returns to normal conditions by the middle of year +1. That is, in October +1 the western Pacific thermocline deepens and in the central and eastern Pacific the thermocline shoals, removing completely the warm water layer of El Niño February +1. FIG. 6.

The changes to the equatorial warm water layer thickness of the 1990's composite El Niño are similar to the variations in the depth of the 20°C isotherm discussed by Meinen and McPhaden (2001). The analysis of Meinen and McPhaden (2001) is based on observations from which the seasonal variability is removed and a 5-month running filter is applied to the mean. As such, their study represents the low-frequency response of the thermocline during an El Niño event. Therefore, while the present inverse model EUC velocity estimates are biased towards the high-frequency El Niño component, the equatorial thermocline slope is representative of the El Niño low-frequency component.

Note that the composite El Niño suggests a pivot point for the warm water volume of ≈170°W (Fig. 6). This coincides with the longitude division between the western and central Pacific based on the mean zonal equatorial thermocline slope in Sloyan et al. (2003). Wyrtki (1985) and Meinen and McPhaden (2001), however, found the warm water pivot point further

east at ≈155°W.

In February +0 of the 1990's composite El Niño the SOI has just begun its negative trend (Fig. 1), the equatorial thermocline slope has not relaxed, and the zonal current transports (Fig. 4) are the same as their mean seasonal value within model errors. Therefore, February +0 reflects the normal seasonal conditions. February +1 is representative of the El Niño mature phase. The SEC(N,S) transport are anomalously low in the western and central Pacific, and the zonal thermocline slope is relaxed. Anomalous NECC and EEC eastward surface transport are found at February +1 in the western and central Pacific.

A comparison of the tropical Pacific circulation between El Niño February +0 and +1 reveals changes in the equatorial circulation between the seasonal mean and the mature phase of the composite El Niño, but the aliasing of the EUC must be kept in mind.

1) Western Region

In the western Pacific the southern and western boundaries of the model step around the islands of Papua New Guinea (Fig. 2). The northward and eastward transports across these boundaries are associated with several branches of the southern hemisphere low-latitude western boundary currents (Butt and Lindstrom 1994; Lukas et al. 1996). The equatorward transport across 3°S is associated with the New Guinea Coastal Current (NGCC) and a branch of the New Guinea Coastal Undercurrent (NGCUC) (Lukas et al. 1996), which flows directly onto the equator in the far west. The NGCUC results in a net transport onto the equator across these boundaries in February +0 and +1 (Fig. 7 a and b). [Note that in Fig. 7 the combined equatorward transport at 3°S, 5°S and 8°S, is shown for simplicity at 8°S. The net transport at 8°S in Fig. 7 is dominated by equatorward transport of the NGCUC at 3°S.] The northward transport of the NGCUC across the southern boundary of the model at 3°S at El Niño onset and mature phases is similar. There is, however, weak anomalous eastward transport at the western boundary between 8°S and 2°S in February +1 compared to February +0 (Fig. 7 c). This anomalous eastward transport is associated with an increase of the NGCUC adjacent to

New Ireland (156°E, eastern island of the Bismarck Archipelago) from 3 ± 2 Sv at February +0 to 13 ± 2 Sv at February +1. This anomalous transport may result from a transport increase of the NGCUC south of 3°S, that rather than passing through the Vitiaz Strait is deflected to the east via the Solomon Strait leading to enhanced equatorward transport at the eastern branch of the NGCUC (Fine et al. 1994). FIG. 7.

Much of the transport associated with the southern hemisphere low latitude western boundary current flows directly out of the region across 143°E (Fig. 7) with anomalous westward transport between February +1 and February +0 associated with the increased transport of the NGCUC. The current retroflects towards the equator in the far western Pacific, and together with eastward transport from the Mindanao Current feeds the transport at 156°E between 2°N and 8°N (Fine et al. 1994; Sloyan et al. 2003). The eastward transport across 156°E doubles between February +0 (23 ± 3 Sv) and February +1 (47 ± 5 Sv). The anomalous NGCUC cross-equator transport accounts for approximately half of this increase, the Mindanao Current, that also feeds the eastward transport at 156°W, must account for the remaining transport increase.

At 170°W, between 8°S and 2°N, westward transport of the SEC(S) decreases between February +0 and +1 resulting in an anomalous eastward surface transport in the southern and equator sectors. A small reduction in the strength of the EUC results in anomalous westward transport in the equator sector. The increased eastward transport of the northern and southern low latitude boundary currents in February +1 results in anomalous eastward transport at 170°W between 2°N and 8°N.

Anomalous poleward transport across the surface and upper thermocline layers at 8°N, 2°N and 2°S between February +0 and February +1 (Fig. 7). Off-equatorial Ekman transport is reduced in February +1 with respect to February +0 (Table 2). Therefore, the anomalous meridional transport is due to reduced equatorward geostrophic flow. This finding is in agreement with Jin's 1997a; 1997b warm water discharge hypothesis. Anomalous equatorward transport of lower thermocline water at $\pm 2^\circ$ results from the transport increase

of the low latitude western boundary currents.

Differences in the estimated diapycnal transports between composite El Niño February +1 and February +0 are closely related to anomalous horizontal transports at the boundaries of the western region. The anomalous equatorward transport in the NGCUC, and anomalous surface poleward transport at 2°S drive anomalous downwelling between 8°S and 2°S. Anomalous low latitude western boundary current transport onto the equator drives anomalous upwelling from the thermostad to lower thermocline in the equatorial sector. In the northern sector (2°N-8°N) anomalous downwelling is found across the upper and lower thermocline layers due to the slowdown in the shallow tropical circulation cell and increased eastward transport from the low latitude western boundary current, respectively.

2) Central Region

In the central Pacific the relaxation of the zonal thermocline slope relates to reduced geostrophic equatorward transport and thus anomalous poleward transport in the subsurface layers across $\pm 8°$ and $\pm 2°$ of latitude (Fig. 7). Across 2°S and 2°N a decrease in the poleward Ekman transport (Table 2) results in an anomalous net equatorward transport in the surface/mixed layer. At 170°W and 125°W (between 8°S and 8°N) both westward and eastward anomalous zonal transports are found. The surface/mixed layer eastward transport anomalies are associated with the movement of the western Pacific warm pool to the central Pacific, and an anomalously strong NECC at February +1. The eastward surface layer and NECC transport anomalies are largest at 170°W. Changes to the meridional (geostrophic and Ekman) transport between February +0 and +1 are balanced in the model by large anomalous diapycnal transports across the upper thermocline layer between 8°S and 8°N (Fig. 7).

Diapycnal and meridional transports at February +0 are similar to those found in a study of the mean tropical Pacific (Sloyan et al. 2003). In the central Pacific, upwelling across the outcropping surface mixed layer (16 ± 4 Sv), surface layer poleward transport across $\pm 2°$, off-equatorial downwelling, and subsurface equatorward transport across $\pm 2°$ are components

of the shallow tropical circulation cell (Fig. 7). Anomalies between February +1 and February +0 show that equatorial upwelling of upper thermocline water to the surface/mixed layer ceases, resulting in anomalous downwelling, while the off-equatorial diapycnal transport reverses and anomalous upwelling occurs in the northern and southern sectors. The direction of the diapycnal transports across the lower thermocline and thermostad layers is consistent between February +1 and February +0 but anomalous downwelling in the northern and equatorial sectors, and upwelling in the southern sector of O(2 Sv) exist.

Changes to the zonal, meridional and diapycnal transports in the surface and upper thermocline layer significantly affect the shallow tropical overturning cell and EUC transport. During the mature phase of El Niño the relaxation of the thermocline slope corresponds to a reduction in the lower limb of the shallow tropical cell and upwelling of upper thermocline water to the surface ceases. The inverse model suggests that the cessation of cool upper thermocline water upwelling to the surface layer, and eastward advection from the western Pacific warm pool are significant factors that result in the warming of the surface waters of the central Pacific. Absent or limited upwelling from the EUC upper thermocline allows the EUC transport in this layer to be maintained across the central Pacific. The sporadic eastward transport along the equator by the Kelvin waves is not removed from the EUC by upwelling, but flows relatively unchanged across the equatorial Pacific (see Section 5).

3) Eastern Region

In contrast to the central Pacific, smaller meridional transport anomalies of approximately 1-2 Sv are found across latitudes $\pm 8^\circ$ and $\pm\ 2^\circ$ (Fig. 7). Ekman transport at February +0 and February +1 are similar (Table 2). The (small) anomalous poleward transport in the thermostad layer at 8°S and 8°N is due to increased poleward transport between 125°W and 95°W, and is not associated with poleward transport along the eastern boundary.

At 95°W, anomalous westward transport of warm surface/mixed layer water is seen. This and anomalous eastward transport of surface water at 125°W in the equatorial sector result

in a continuous layer of warm surface water across the entire equatorial Pacific at the mature phase of the 1990's composite El Niño cycle. Diapycnal transports across the upper and lower thermocline at February +1 have the same structure as February +0 but are generally 2 to 3 Sv larger (Fig. 7).

The most significant anomalous transport, zonal and diapycnal, between February +1 and February +0 is associated with the thermostad layer. At 95°W, anomalous eastward transport of EUC thermostad water occurs. In February +0 diapycnal downwelling between the lower thermocline and thermostad was found, while at February +1 no diapycnal transport between these layers occurs. This results in anomalous upwelling between the lower thermocline and thermostad layers. The changes in the diapycnal transport between the lower thermocline and thermostad layers and EUC transport in these layers balance the storage term in (1). This increases the thickness of these layers during the mature and decay phase of the El Niño cycle.

The February +0 and +1 circulation of the eastern Pacific is different from the mean circulation (Sloyan et al. 2003). In February +0, downwelling from the lower thermocline to the thermostad occurs, while in the mean circulation upwelling from the thermostad through to the surface layer is found. The difference between February +0 and the mean circulation may indicate that the termination of the EUC and strength of the cold tongue are influenced by the seasonal cycle. The circulation at February +0 suggests that at this time upwelling is limited to the upper 100 m of the eastern Pacific and downwelling occurs between the lower thermocline and thermostad layers of the EUC. This shutdown of upwelling of cold EUC thermostad water during February results in a warming of the cold tongue sea-surface temperature. At this time of the year the EUC lower thermocline and thermostad layers terminate by poleward transport in the eastern Pacific and adjacent to the Americas (Lukas 1986).

5. Impact of the high-frequency El Niño component on the Equatorial Pacific circulation.

The maintenance of the EUC during the composite El Niño results from a bias in the timing of the CTD/ADCP surveys, that (unfortunately) were mostly taken when westerly wind anomalies briefly restored EUC velocities to near-normal values. These enhanced eastward velocities as the Kelvin waves travel along the equator are found in the subsurface EUC water layers as well as the surface layer. Inverse model EUC upper and lower thermocline layer velocities at the equator, however, are not dramatically different from the mean ADCP EUC layer velocities from the TAO equatorial moorings (Fig. 8). Thus the inverse model does not significantly over-estimate the net EUC transport for the composite El Niño cycle. FIG. 8.

During the El Niño cycle, the aliased sampling of high-frequency eastward velocities (Fig. 5) makes it appear that the EUC transport continues at near-normal values. At these times, however these data can still speak to the El Niño low-frequency thermocline signature (Fig. 9). Eastward transport pulses at the onset and transition phases of El Niño traverse the equatorial Pacific as the zonal thermocline slope is just beginning to relax. At this time, in the central and eastern Pacific, the eastward transport pulses within the upper and lower thermocline and thermostad layers occur when these layers still shoal and outcrop to the east (Feb.+0, Fig. 9), and SEC transport is at near normal values (Feb +0, Fig. 4). The shoaling of the EUC and surface westward velocity result in mixing (Feb. +0, Fig. 7), either by direct air-sea forcing and/or the strong vertical shear between the mixed layer and EUC, that may act to redistribute the high-frequency EUC transport pulses. However, high-frequency EUC transport pulses at the mature and decay phases of the El Niño cycle occur when the thermocline is deep in the central and eastern Pacific (Feb. +1 and June +1, Fig. 9) and surface eastward equatorial transport is found across the equatorial Pacific (Feb +, Fig. 4). The deepening of the thermocline isolates the EUC layers from surface forcing and the eastward surface velocity result in a reduced vertical shear between the mixed layer and EUC. These changes to the zonal thermocline slope and vertical velocity shear act to reduce mixing

between the EUC and surface/mixed layer (Feb +1, Fig. 4), thereby limiting the redistribution of the EUC transport pulses. Essentially the El Niño low-frequency thermocline response may influence how the equatorial Pacific redistributes the high-frequency EUC transport variability. At the mature and decay El Niño phases, the EUC transport pulses in the upper and lower thermocline and thermostad layers are able to traverse the equatorial Pacific relatively unchanged resulting in a mass convergence in the eastern Pacific. FIG. 9.

The inverse model suggests that the pulses of eastward EUC transport during the mature and decay phases of the El Niño cycle may modify the eastern equatorial Pacific thermocline. In the eastern Pacific, anomalous poleward transport across 8°S and 8°N adjacent to the Americas coast does not accompany the lower thermocline and thermostad EUC transport pulses at 95°W. The EUC transport pulses increase the volume (thickness) of thermostad and lower thermocline layers within the eastern Pacific (Fig. 9). The depth of the lower boundary of the thermostad layer remains at ≈ 400 m between February +1 and June +1, but its upper boundary rises from 220 m to 200 m. Subsequently, the upper boundary of the lower and upper thermocline layers shoal by approximately 40 to 50 m between the El Niño mature and decay phases. The shoaling of the thermocline results in increased upwelling between the lower and upper thermocline layers in February +1 in comparison to February +0 (Fig. 7). After El Niño sea-surface temperature warming reaches its maximum during the mature phase there is a slow recovery of the subsurface thermocline structure in the eastern Pacific. Recovery of the thermocline involves both the increase in thickness of the upper and lower thermocline layers and thermostad, and/or the shoaling of the thermocline. The high-frequency transport pulses that transverse the equatorial Pacific during El Niño mature and decay phases may be a mechanism through which the eastern Pacific begins to restore the subsurface layer thickness prior to eastern and central Pacific sea-surface cooling that heralds the end of an El Niño event.

A common feature of the final phases of observed El Niño events is that the eastern Pacific thermocline begins to shoal two to three months before the sea-surface temperature cool (Harrison and Vecchi 1999; Kessler and McPhaden 1995b; McPhaden 1999). The

shoaling of the thermocline after peak warming in the El Niño cycle generally occurs in phase with the eastward propagation of the seasonal variation of the 20°C isotherm depth and dynamic height in the central and eastern Pacific (Yu and McPhaden 1999). Simple models of wind forced Rossby and Kelvin wave variability within the equatorial region suggest that the eastward phase speed of the 20°C isotherm depth and dynamic height may be explained by a mix of Kelvin and Rossby waves (Yu and McPhaden 1999). Kessler and McPhaden (1995a) find that interior wind-forced Kelvin waves do not account for the thermocline shoaling in the 1991-1992 El Niño event. Rather, they suggest that westerly wind anomalies in the central Pacific during El Niño mature phase produce upwelling Rossby waves that reflect at the western boundary and cause the shoaling of the thermocline in the central and eastern Pacific. These westerly wind anomalies occurred at or slightly south of the equator in the central Pacific (Kessler and McPhaden 1995b). Harrison and Vecchi (1999), however, find that the southward shift of the wind anomalies directly force thermocline shoaling that is of equal importance to that due to western boundary reflection. They suggest that the southward shift of the westerly wind anomaly results from the normal seasonal cycle, and thus the termination of an El Niño event is linked to the seasonal cycle.

The inverse model does not determine the mechanisms responsible for the thermocline shoaling after peak warming in the central and eastern Pacific. The shoaling, however, is implicitly included through the linked 13 bimonthly potential density sections and water layer storage term in (1). Associated with the shoaling of the thermocline is a thickness increase of the lower thermocline and thermostad layers (Fig. 9). The inverse model suggests that the EUC high-frequency transport pulses may be important in the volume increase of the subsurface layers as the thermocline shoals.

6. Conclusions

The 1990's composite El Niño inverse model, in agreement with studies of individual El Niño events, shows SEC(S/N) transport decreases, NECC transport increase and development of equatorial eastward surface transport in the western and central Pacific. Transport anomalies of the SEC and NECC are the result of changes in the depth of the equatorial thermocline. They are representative of the advective signature of El Niño. EUC transport, however, appears in this dataset to be maintained at near-seasonal values. This erroneous finding results from a bias in the timing of the ADCP surveys. Although the CTD and ADCP surveys adequately sample some features of the 1990's El Niño events, the surveys coincidentally crossed the equator when eastward current pulses briefly return the EUC transport to near-normal values. These are probably the result of Kelvin waves excited by westerly winds anomalies. Their eastward velocity signal is found in the EUC thermocline and thermostad layers and not solely confined to the surface layer.

In the inverse model eastward advection is important in moving the western Pacific warm pool across 170°W, however east of 140°W advection plays a secondary role, and a decrease in diapycnal transport leads to sea-surface warming. This finding agrees with previous studies (Vialard et al. 2001). Although there is a large exchange of warm surface water between the western and central Pacific the thickness of this surface/mixed layer only slightly decreases in the western Pacific. A similar slight shoaling of the 20°C isotherm was noted for previous Los Niños (McPhaden et al. 1990; Meinen et al. 2001). As these studies suggest, we find that the thickness of the surface/mixed layer in the western region is maintained during El Niño by anomalous equatorward transport in the northern and southern low latitude western boundary currents between 3°S and 8°N. In the present study we find that equatorward transport across 3°S associated with the western branch of the NGCUC is unchanged within the given errors (30 ± 15 Sv). There is, however, an increase in the NGCUC transport adjacent to New Ireland (156°E, eastern island of the Bismarck Archipelago) from 3 ± 2 Sv at El Niño onset and decay to 13 ± 2 Sv at El Niño transition and mature stages. This increase may be the

result of increased northward transport of the NGCUC south of 3°S that rather than passing through the Vitiaz Strait is deflected to the east leading to enhanced equatorward transport in the eastern branch of the NGCUC. In the northern hemisphere the eastward transport across 156°E doubles between El Niño onset (23 ± 3 Sv) and mature (47 ± 5 Sv) stages. Approximately half this increase must be due to increased transport from the northern low latitude western boundary current – the Mindanao Current.

During El Niño decreased equatorial upwelling of upper thermocline water to the surface/mixed layer, Ekman poleward transport and subsurface equatorward geostrophic transport across latitudes $\pm 2^{\circ}$ all manifest in a significant slowdown of the shallow tropical overturning cell. In the central and eastern Pacific, at El Niño onset (Feb. +0), the downward limbs of the shallow overturning circulation are 2 ± 6 Sv in the northern (2 to 8°N) sector, and 11 ± 6 Sv in the southern (2 to 8°S) sector, while at the mature El Niño phase (Feb. +1) the downward limb is replaced by net upwelling in the northern (6 ± 6 Sv) and southern (1 ± 6 Sv) sectors. Note also, the difference in the strength of these cells between the mean tropical circulation [15 ± 13Sv in the northern sector and 20 ± 11 Sv in the southern sector, (Sloyan et al. 2003)] and Feb. +0 may reflect the influence of the seasonal cycle on the shallow overturning circulation.

In the central Pacific, anomalous poleward transport across 8°S suggests that during El Niño the interior (basin) pathway is less effective in supplying South Pacific subtropical water to the equator. The reduction of the interior pathway transport (4.5 Sv) is compensated by increased equatorward transport in the NGCUC. This indicates that during El Niño the route by which southern hemisphere subtropical water enters the equatorial Pacific is principally via the low latitude western boundary current.

The high-frequency EUC transport pulses at the El Niño mature phase tend to occur while the equatorial thermocline slope is depressed in the central and eastern Pacific (Kessler 2001). The deeper thermocline results in the cessation of upwelling from the EUC upper thermocline in the central Pacific. Thus EUC transport pulses must travel along the equator to the eastern

Pacific. The inverse model results suggest that in the eastern Pacific the EUC transport pulses may be an important in factor in reestablishing the thermocline depth and sub-surface layer thickness prior to sea-surface cooling that signifies the end of an El Niño event. This study points to the potential influence of the high-frequency El Niño component, and their timing with respect to the seasonal cycle, on restoring the eastern Pacific thermocline depth and layer thickness. These results suggest that El Niño models need to consider the high-frequency velocity response to westerly wind events on El Niño termination.

Acknowledgments. BMS was supported by a National Research Council Research Associateship Award to NOAA's Pacific Marine Environmental Laboratory (PMEL), a Climate and Global Change Program from the NOAA Office of Global Programs, and funds provided by the Woods Hole Oceanographic Institution (WHOI) from the *The James S. Cole and Cecily C. Selby Endowed Fund* and *The Penzance Endowed Fund in Support of Assistant Scientists*. GCJ and WSK were supported by the NOAA Office of Oceanic and Atmospheric Research and the NOAA Office of Global Programs. Comments from John Toole and Kurt Polzin improved the manuscript.

REFERENCES

Baturin, N. G., and P. P. Niiler, 1997: Effects of instability waves in the mixed layer of the equatorial Pacific. *Journal of Geophysical Research*, **102**, 27,771–27,793.

Bryden, H. L., and E. C. Brady, 1985: Diagnostic model of the three–dimensional circulation in the upper equatorial Pacific Ocean. *Journal of Physical Oceanography*, **15**, 1255–1273.

Butt, J., and E. Lindstrom, 1994: Currents off the east coast of New Ireland, Papua New Guinea, and their relevance to the regional undercurrents in the western equatorial Pacific Ocean. *Journal of Geophysical Research*, **99**, 12,503–12,514.

Chelton, D. B., M. G. Schlax, J. M. Lyman, and G. C. Johnson, 2003: Equatorially trapped Rossby waves in the presence of meridionally sheared baroclinic flow in the Pacific Ocean . *Progress in Oceanography*, **52**, 323–380.

Delcroix, T., G. Eldin, M.-H. Radenac, J. Toole, and F. E., 1992: Variation of the western equatorial Pacific Ocean, 1986-1988. *Journal of Geophysical Research*, **97**, 5423–5445.

Delcroix, T., B. Dewitte, Y. duPenhoat, F. Masia, and J. Picaut, 2000: Equatorial waves and warm pool displacements during the 1992-1998 El Niño Southern Oscillation events: Observation and modeling. *Journal of Geophysical Research*, **105**, 26,045–26,062.

Fine, R. A., R. Lukas, F. M. Bingham, M. J. Warner, and R. H. Gammon, 1994: The western equatorial Pacific: A water mass crossroads. *Journal of Geophysical Research*, **99**, 25,063–25,080.

Firing, E., R. Lukas, J. Sadler, and K. Wyrtki, 1983: Equatorial Undercurrent disappears during the 1982-1983 El Ni no. *Science*, **222**, 1121–1123.

Gouriou, Y., and T. Toole, 1993: Mean circulation of the upper layers of the western equatorial Pacific Ocean. *Journal of Geophysical Research*, **98**, 22,495–22,520.

Halpern, D., 1987: Observations of annual and El Niño thermal and flow variations at 0°, 110°W and 0°, 95°W during 1980-1985. *Journal of Geophysical Research*, **92**, 8197–8212.

Hansen, D. V., and C. A. Paul, 1984: Genesis and effects of long waves in the equatorial Pacific. *Journal of Geophysical Research*, **89**, 10,431–10.440.

Harrison, D. E., and G. A. Vecchi, 1999: On the termination of El Niño. *Geophysical Research Letters*, **26**, 1593–1596.

Hayes, S. P., J. M. Toole, and L. J. Mangum, 1983: Water-mass and transport variability at 110°W in the equatorial Pacific. *Journal of Physical Oceanography*, **13**, 153–168.

Jin, F.-F., 1997a: An equatorail ocean recharge paradigm for ENSO. Part I: Conceptual model. *Journal of Atmospheric Sciences*, **54**, 811–829.

Jin, F.-F., 1997b: An equatorail ocean recharge paradigm for ENSO. Part II: A stripped-down coupled model. *Journal of Atmospheric Sciences*, **54**, 830–847.

Johnson, G. C., M. J. McPhaden, G. D. Rowe, and K. E. McTaggart, 2000: Upper equatorial Pacific Ocean current and salinity variability during the 1996-1998 El Niño—La Niña cycle. *Journal of Geophysical Research*, **105**, 1037–1053.

Johnson, G. C., M. J. McPhaden, and E. Firing, 2001: Equatorial Pacific Ocean horizontal velocity, divergence and upwelling. *Journal of Physical Oceanography*, **31**, 839–849.

Johnson, G. C., B. M. Sloyan, W. S. Kessler, and K. E. McTaggart, 2002: Direct measurements of upper ocean currents and water properties across the tropical Pacific during the 1990's. *Progress in Oceanography*, **52**, 31–61.

Kessler, W. S., 2001: EOF representation of the Madden-Julian Oscillation and its connection with ENSO. *Journal of Climate*, **14**, 3055–3061.

Kessler, W. S., and M. J. McPhaden, 1995a: Oceanic equatorial waves and the 1991-93 El Niño. *Journal of Climate*, **8**, 1757–1774.

Kessler, W. S., and M. J. McPhaden, 1995b: The 1991-1993 El Niño in the central Pacific. *Deep–Sea Res. II*, **42**, 295–333.

Kessler, W. S., and B. A. Taft, 1987: Dynamic heights and zonal geostrophic transports in the central tropical Pacific during 1979-84. *Journal of Physical Oceanography*, **17**, 97–122.

Kessler, W. S., L. M. Rothstein, and D. Chen, 1998: The annual cycle of SST in the eastern tropical Pacific, as diagnosed in an ocean GCM. *Journal of Climate*, **11**, 777–799.

Lagerloef, G. S. E., G. T. Mitchum, R. G. Lukas, and P. P. Niiler, 1999: Tropical Pacific near-surface currents estimated from altimeter, wind, and drifter data. *Journal of Geophysical Research*, **104**, 23,313–23,326.

Lukas, R., 1986: The termination of the equatorial undercurrent in the eastern Pacific. *Progress in Oceanography*, **16**, 63–90.

Lukas, R., T. Yamagata, and J. P. McCreary, 1996: Pacific low-latitude western boundary currents and the Indonesian throughflow. *Journal of Geophysical Research*, **101**, 12,209–12,216.

McPhaden, M. J., 1999: Genesis and evolution of the 1997-98 El Niño. *Science*, **283**, 950–954.

McPhaden, M. J., and S. P. Hayes, 1990: Variability in the eastern equatorial Pacific Ocean during 1986-1988. *Journal of Geophysical Research*, **95**, 13,195–13,208.

McPhaden, M. J., S. P. Hayes, L. J. Mangum, and J. M. Toole, 1990: Variability in the western equatorial Pacific during the 1986-87 El Niño/Southern Oscillation event. *Journal of Physical Oceanography*, **20**, 190–208.

Meinen, C. S., and M. J. McPhaden, 2001: Interannual variability in warm water volume transport in the equatorial Pacific during 1993-99. *Journal of Physical Oceanography*, **31**, 1324–1345.

Meinen, C. S., M. J. McPhaden, and G. C. Johnson, 2001: Vertical velocities and transports in the equatorial Pacific during 1993–1999. *Journal of Physical Oceanography,* **31**, 3230–3248.

Picaut, J., M. Ioualalen, C. Menkes, D. T., and M. J. McPahaden, 1996: Mechanism of the zonal displacement of the Pacific warm pool: Implications for ENSO. *Science,* **274**, 1486–1489.

Picaut, J., M. Ioualalen, D. T., F. Masia, R. Murtugudde, and J. Vialard, 2001: The oceanic zone of convergence on the eastern edge of the Pacific warm pool: A synthesis of results and implications for El Niño-Southern Oscillation and biogeochemical phenomena. *Journal of Geophysical Research*, **106**, 2363–2386.

Picaut, J., E. Hackert, A. J. Busalacchi, R. Murtugudde, and G. S. E. Lagerloef, 2002: Mechanisms of the 1997-1998 El Niño-La Niña, as inferred from space-based observations. *Journal of Geophysical Research*, **107(C5)**, 10.1029/2001JC000,850.

Rasmusson, E., and T. H. Carpenter, 1982: Variations in tropical sea surface temperature and surface wind fields associated with the Southern Oscillation/El Niño. *Monthly Weather Review*, **110**, 354–384.

Reverdin, G., C. Frankignoul, E. Kestenare, and M. J. McPhaden, 1994: Seasonal variability in the surface currents of the equatorial Pacific. *Journal of Geophysical Research*, **99**, 20,323–20,344.

Sloyan, B. M., G. C. Johnson, and W. S. Kessler, 2003: The Pacific cold tongue: A pathway for interhemispheric exchange. *Journal of Physical Oceanography*, **33**, 1027–1043.

Taft, B. A., and W. S. Kessler, 1991: Variations of zonal currents in the central tropical Pacific during 1970 to 1987: Sea level and dynamic height measurements. *Journal of Geophysical Research*, **96**, 12,599–12,618.

Toole, J. M., and M. D. Borges, 1984: Observations of horizontal and vertical displacements

in the equatorial Pacific ocean associated with the early stages of the 1992/83 El Niño. *Journal of Physical Oceanography*, **14**, 984–959.

Vialard, J., C. Menkes, J.-P. Boulanger, P. Delecluse, E. Guilyardi, M. McPhaden, and G. Madec, 2001: A model study of oceanic mechanisms affecting equatorial Pacific sea surface temperture during the 1997-98 El Niño. *Journal of Physical Oceanography*, **31**, 1649–1675.

Wang, B., 1995: Interdecadal changes in El Niño onset in the last four decades. *Journal of Climate*, **8**, 267–285.

Wang, C., and R. H. Weisberg, 2000: The 1997-98 El Niño evolution relative to previous El Niño events. *Journal of Climate*, **13**, 488–501.

Weisberg, R. H., and L. Qiao, 2000: Equatorial upwelling in the central Pacific estimated from moored velocity profilers. *Journal of Physical Oceanography*, **30**, 105–124.

Wunsch, C., 1996: *The Ocean Circulation Inverse Problem*. Cambridge University Press,.

Wyrtki, K., 1975: El Niño- The dynamical response of the equatorial Pacific Ocean to atmospheric forcing. *Journal of Physical Oceanography*, **5**, 572–584.

Wyrtki, K., 1981: An estimate of equatorial upwelling in the Pacific. *Journal of Physical Oceanography*, **11**, 1205–1214.

Wyrtki, K., 1985: Water displacements in the Pacific and genesis of El Niño cycles. *Journal of Geophysical Research*, **90**, 7129–7132.

Yu, X., and M. J. McPhaden, 1999: Seasonal variability in the equatorial Pacific. *Journal of Physical Oceanography*, **29**, 925–947.

Printed July 20, 2004.

Figure Captions

FIG. 1. SOI during each individual El Niño event for the observational period of this study and their mean.

FIG. 2. Position of zonal and meridional boundaries (dashed lines) and the box (25) regions used in this study. The boundaries are formed from a combination of CTD and ADCP data (Johnson et al. 2002) and historical CTD and XBT data in the eastern Pacific.

FIG. 3. Current transport ($\times 10^6$ m^3 s^{-1}) from the mean seasonal cycle (SOI=0) in the tropical Pacific as a function of longitude and month. The mean seasonal current transports are calculated from the CTD and ADCP data (Johnson et al. 2002). Eastward is positive.

FIG. 4. Current transport ($\times 10^6$ m^3 s^{-1}) during the composite El Niño (left panel) and anomaly (right panel) from the mean seasonal cycle in the tropical Pacific as a function of longitude and bimonthly composite El Niño cycle. El Niño transport anomalies are deviations from the transport of the mean seasonal current (SOI=0), calculated from the CTD and ADCP data (Johnson et al. 2002). Eastward is positive, and positive anomalies in the direction of the mean current.

FIG. 5. Vertically (0-250m) average 15-day smoothed time-series of ADCP zonal current anomalies (solid black line, cm s^{-1}) from TAO equatorial moorings at 165°E, 170°W, 140°W and 110°W. Also shown is the five month running mean SOI (green line). Red vertical lines show equator crossing dates of CTD/ADCP cruises used in this study to produce the 24-month composite El Niño cycle.

FIG. 6. Thickness (m) difference during El Niño of water lighter than $\sigma_\theta \leq 25.5$ kg m^{-3} between (a) February +0 and +1, and (b) October +0 and +1. The pivot point of the warm water volume in the tropical Pacific between 8°S and 4°N is located at ≈ 170°W, while north of 4°N the pivot point extends eastward to 125°W. The $\sigma_\theta = 25.5$ kg m^{-3} surface corresponds approximately to the 20°C isotherm.

FIG. 7. Circulation ($\times 10^6$ m^3 s^{-1}) of the tropical Pacific for the 1990's composite El Niño at a) February +0, b) February +1 and c) the anomaly between February +1 and +0. The tropical Pacific Ocean is divided in 3 regions: western (western boundary-170°W); central (170°W-125°W); and eastern (125°W-eastern boundary). Ekman and geostrophic transports are combined in the meridional transport estimates. Lateral ($\pm 8^\circ$ green and $\pm 2^\circ$ red) and zonal (black) transports are indicated by solid arrows. Lateral transports at $\pm 2^\circ$ are shown on the western boundary of each region. Diapycnal transport between layer interfaces for southern, equator and northern sectors are shown on eastern boundary of each region. Only transports and anomalies greater than 1×10^6 m^3 s^{-1}are shown. Water classes are separated by bounding isopycnals surfaces – surface/mixed layer (red), upper thermocline (green), lower thermocline (blue), and thermostad (pink). Note that for the western Pacific, although the southern boundary is shown at 8°S for simplicity, it is actually found over a range of latitudes. Similarly the zonal transport of the western boundary of this region is over a range of longitudes but for simplicity is shown at 156°E. In the eastern Pacific the transport across the bounding sections that close the region at $\pm 8^\circ$ to the American coast are combined with transport estimates between 125°W and 95°W at $\pm 8^\circ$. Sections at $\pm 2^\circ$ are between 125°W and 95°W. The diapycnal transports for the region between 95°W and the American coast are folded into the equatorial sector, between 125°W and 95°W.

FIG. 8. EUC upper and lower thermocline vertically averaged velocities of the 60-day smoothed time-series ADCP zonal velocities from the TAO equatorial moorings at 140°W and 110°W for each individual El Niño event of the observation period of this study and their mean. The 13-bimonthly El Niño inverse model EUC upper and lower thermocline velocities (filled square) on the equator ($\pm 0.2°$) are also shown for the event cycle. Upper and lower thermocline water classes are as defined Table 1, and EUC as defined in Table 3.

FIG. 9. Evolution of the thermocline structure in the central and eastern Pacific at 155°W, 125°W and 95°W from the onset (Feb. +0) to mature (Feb. +1) and decay (June +1) phases of the composite El Niño cycle. By June +1 the zonal thermocline slope has returned to normal. Subsequent Ekman upwelling in the central and eastern Pacific results in a sea-surface temperature cooling that signal the termination of El Niño. Water classes are as in Fig. 7.

Tables

TABLE 1. Isopycnal surfaces and depths that define the 12 layers of the inverse model. The 12 layers are grouped into four general water classes, whose average thickness is given.

Model surface	σ_θ (kg m^{-3})	Model Layer	Water Class	Thickness (m)
	surface			
1	21.3	1	Surface	
2	21.7	2	and	30
3	22.5	3	Mixed	
4	23.0	4	Layer	
	23.0		Upper	
5	24.0	5	Thermocline	120
6	25.5	6	water	
	25.5		Lower	
7	26.1	7	Thermocline	70
8	26.3	8	Water	
	26.3			
9	26.5	9	Thermostad	
10	26.7	10	Water	230
11	26.85	11		
12	495 m	12		

Table 1: Bimonthly El Niño Ekman transport ($\times 10^6$ m^3 s^{-1}) estimates across nominally 8°S, 2°S, 2°Nand 8°N for the western (western boundary ñ 170°W), central (170°Wñ 125°W) and eastern (125°Wñ eastern boundary) tropical Pacific regions. The Ekman transport 3°S and 5°S in the western sector are included in the 8°Stransport estimates. Positive is northwards.

El Niño	Western				Central				Eastern			
Cycle	8°S	2°S	2°N	8°N	8°S	2°S	2°N	8°N	8°S	2°S	2°N	8°N
Dec -1	0.17	-3.86	7.64	8.41	-8.90	-26.06	27.56	10.71	-11.92	-11.16	9.07	3.17
Feb +0	1.18	-3.51	10.97	15.38	-6.34	-18.12	21.82	20.10	-10.00	-6.65	5.12	8.33
Apr +0	-0.42	-2.48	6.88	12.51	-6.59	-14.11	14.73	15.89	-10.97	-7.36	4.46	3.65
Jun +0	-4.37	-2.00	2.26	4.63	-10.19	-17.45	12.81	5.10	-14.15	-13.03	7.44	-0.40
Aug +0	-6.49	-1.69	0.79	1.25	-12.49	-24.66	17.39	1.49	-16.12	-19.62	11.90	-3.45
Oct +0	-1.26	-0.22	-0.38	1.15	-9.13	-23.10	18.38	2.18	-14.02	-18.62	11.71	-0.45
Dec +0	1.02	0.39	1.14	5.28	-6.00	-16.89	16.82	8.10	-10.64	-11.79	7.53	3.03
Feb +1	2.35	0.76	2.37	10.96	-3.94	-10.29	12.36	17.06	-8.75	-7.12	3.98	8.54
Apr +1	-0.14	-1.12	4.21	11.16	-5.62	-11.61	12.01	15.01	-10.54	-7.52	4.11	3.69
Jun +1	-5.10	-3.74	4.03	5.45	-11.46	-20.14	15.42	5.65	-14.59	-12.38	7.87	-0.42
Aug +1	-8.41	-5.70	4.15	2.25	-15.61	-31.45	23.96	2.48	-17.14	-18.72	13.10	-3.63
Oct +1	-2.70	-4.18	4.22	2.69	-12.88	-32.60	28.46	3.93	-15.39	-17.84	13.48	-0.45
Dec +1	0.19	-3.68	7.34	8.31	-8.80	-25.73	27.18	10.63	-11.88	-11.18	9.02	3.16

TABLE 3. Zonal current definitions used in this study. SEC is defined as westward transport within given density range, and the remaining zonal currents are eastward transport within their given density ranges.

Current	Latitude Range	Potential Density (σ_θ kg m^{-3})	Comments
SEC	8°S to 2-3°N	$\sigma_\theta \leq 26.3$	SEC(S) 8°S-0°, and SEC(N) 0°-2-3°N
EUC	$\pm 2^\circ$ of equator	$23.0 \leq \sigma_\theta \leq 26.3$	east of 110°W density range extends to $\sigma_\theta \leq 26.7$
SCCs	poleward of $\pm 2^\circ$ and/or equatorward of $\pm 2^\circ$	$\sigma_\theta \geq 25.5$ $\sigma_\theta \geq 26.3$	southern SCC (SSCC) northern SCC (NSCC)
NECC	north of 2.4°N	$\sigma_\theta \leq 25.5$	entire NECC not sampled in east due to 8°N boundary
EEC	$\pm 2^\circ$ of equator	$\sigma_\theta \leq 23.0$	distinguished from EUC by vertical minimum in velocity

Figures

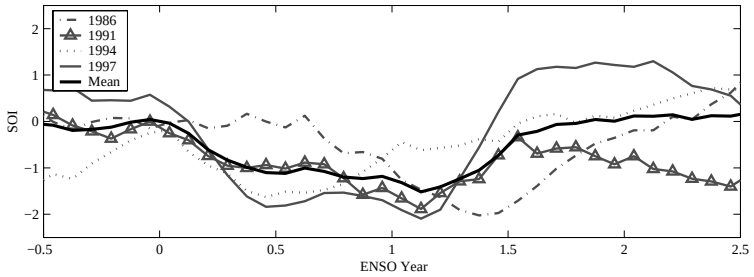

FIG. 1. SOI during each individual El Niño event for the observational period of this study and their mean.

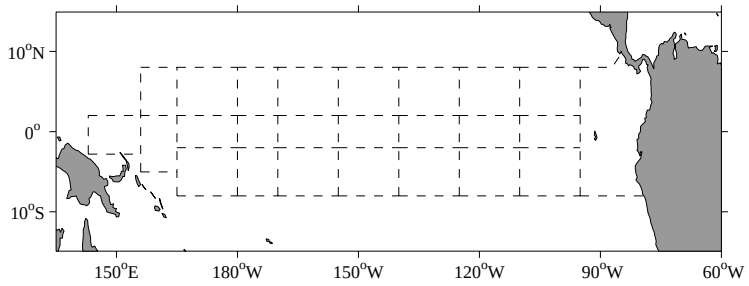

FIG. 2. Position of zonal and meridional boundaries (dashed lines) and the box (25) regions used in this study. The boundaries are formed from a combination of CTD and ADCP data (Johnson et al. 2002) and historical CTD and XBT data in the eastern Pacific.

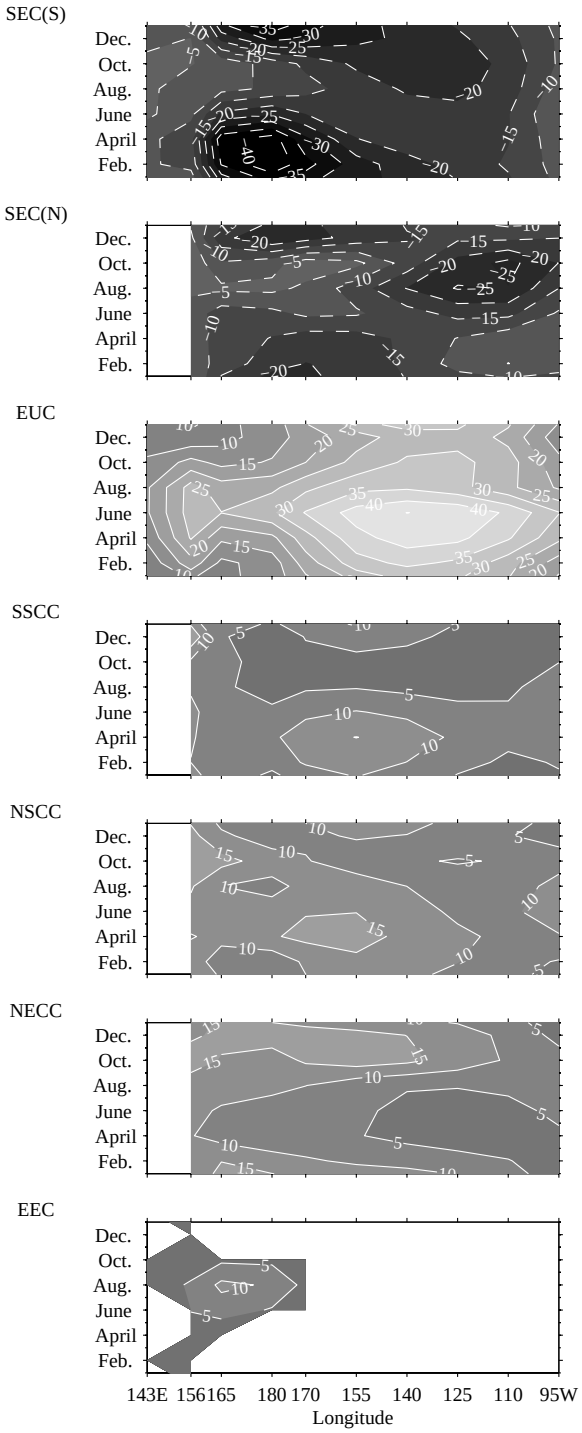

FIG. 3. Current transport ($\times 10^6$ m^3 s^{-1}) from the mean seasonal cycle (SOI=0) in the tropical Pacific as a function of longitude and month. The mean seasonal current transports are calculated from the CTD and ADCP data (Johnson et al. 2002). Eastward is positive.

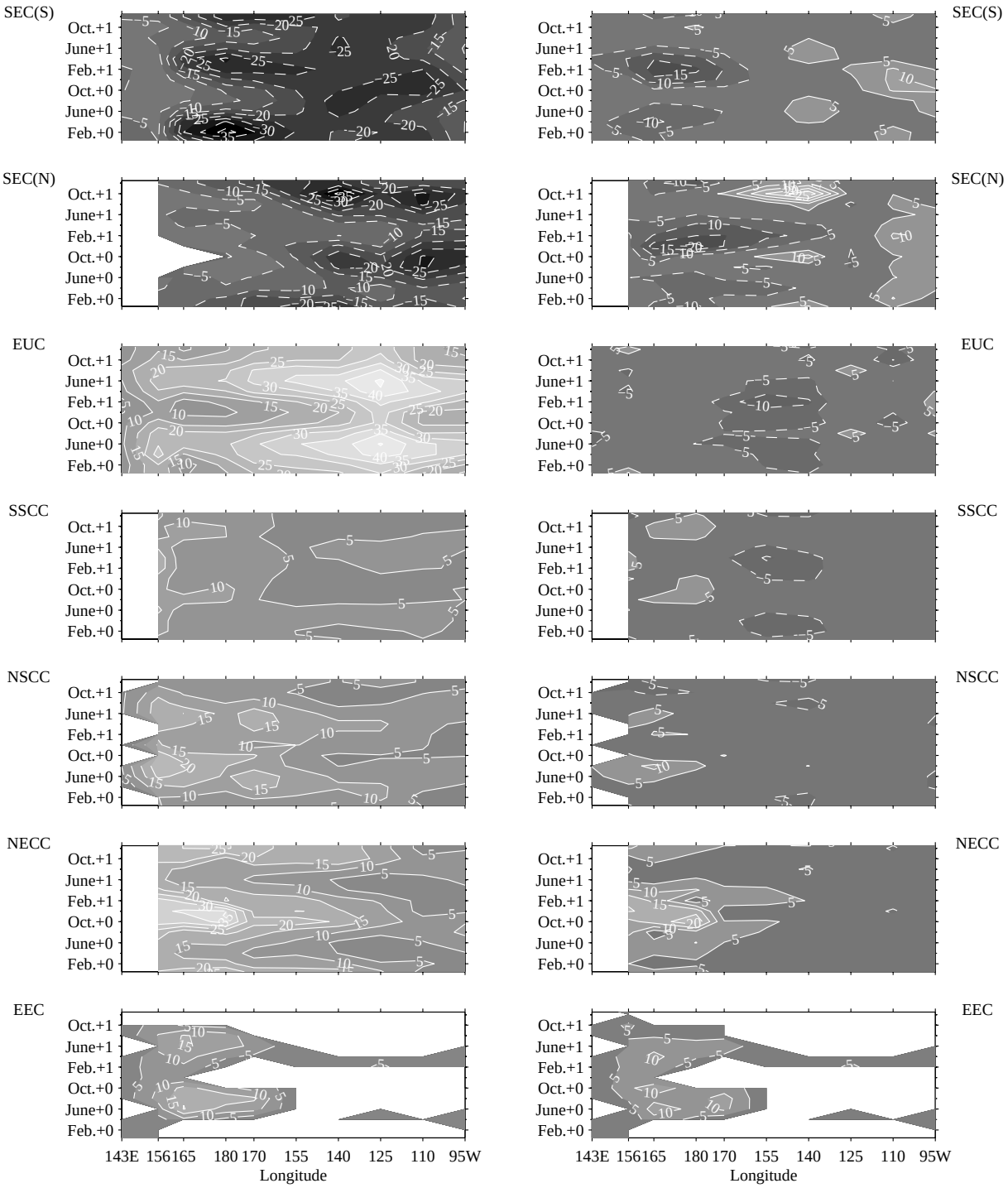

FIG. 4. Current transport ($\times 10^6$ m^3 s^{-1}) during the composite El Niño (left panel) and anomaly (right panel) from the mean seasonal cycle in the tropical Pacific as a function of longitude and bimonthly composite El Niño cycle. El Niño transport anomalies are deviations from the transport of the mean seasonal current (SOI=0), calculated from the CTD and ADCP data (Johnson et al. 2002). Eastward is positive, and positive anomalies in the direction of the mean current.

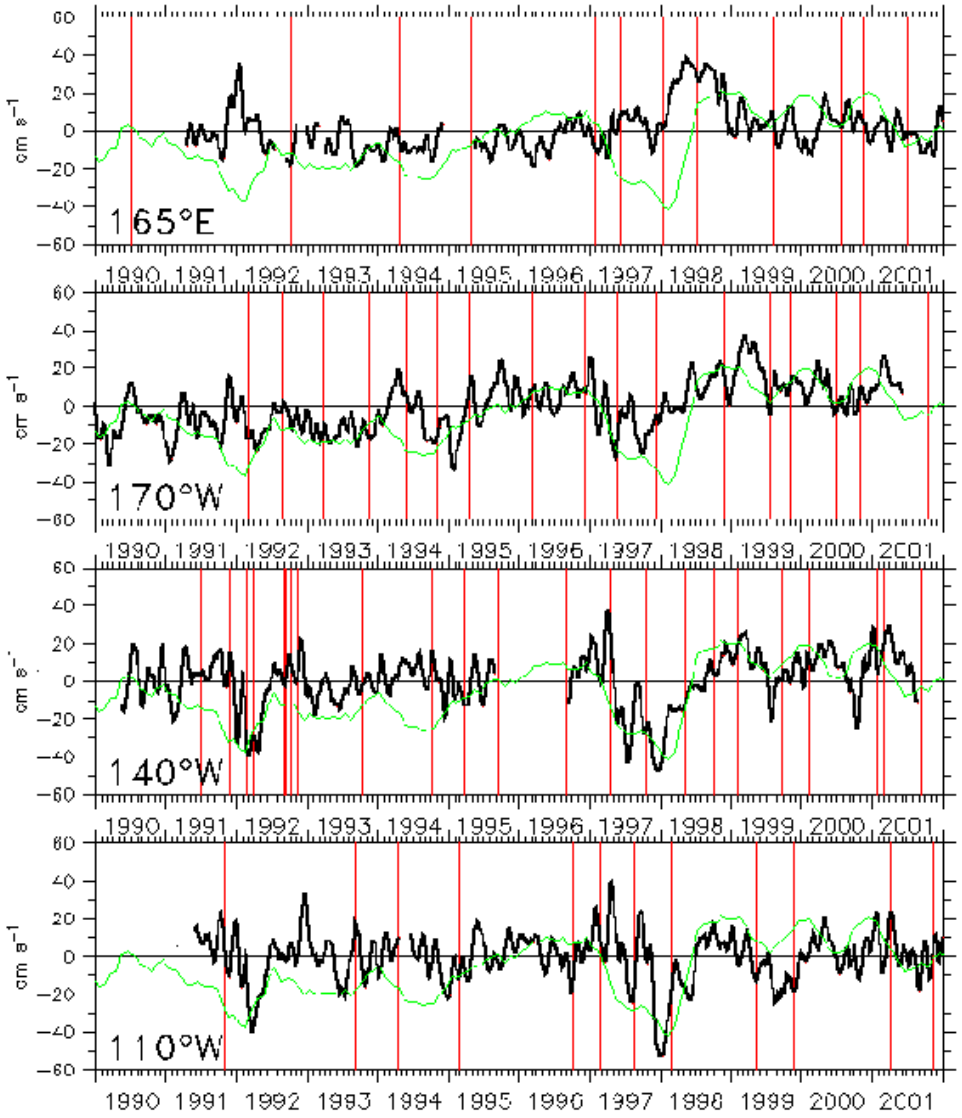

FIG. 5. Vertically (0-250m) average 15-day smoothed time-series of ADCP zonal current anomalies (solid black line, cm s^{-1}) from TAO equatorial moorings at 165°E, 170°W, 140°W and 110°W. Also shown is the five month running mean SOI (green line). Red vertical lines show equator crossing dates of CTD/ADCP cruises used in this study to produce the 24-month composite El Niño cycle.

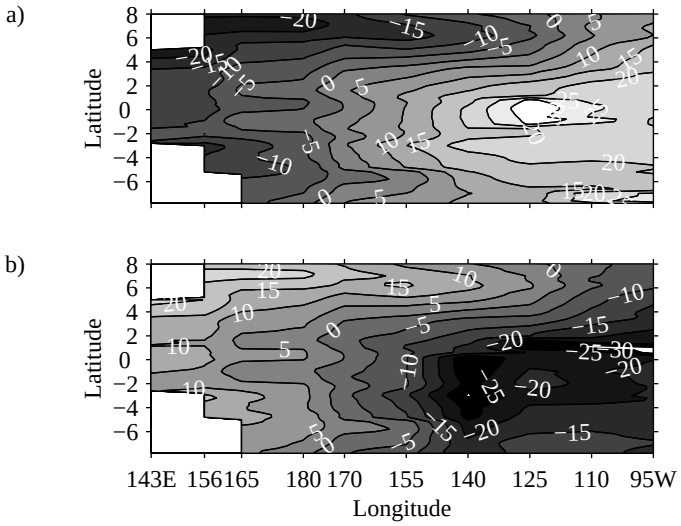

FIG. 6. Thickness (m) difference during El Niño of water lighter than $\sigma_\theta \leq 25.5$ kg m^{-3} between (a) February +0 and +1, and (b) October +0 and +1. The pivot point of the warm water volume in the tropical Pacific between 8°S and 4°N is located at ≈ 170°W, while north of 4°N the pivot point extends eastward to 125°W. The $\sigma_\theta = 25.5$ kg m^{-3} surface corresponds approximately to the 20°C isotherm.

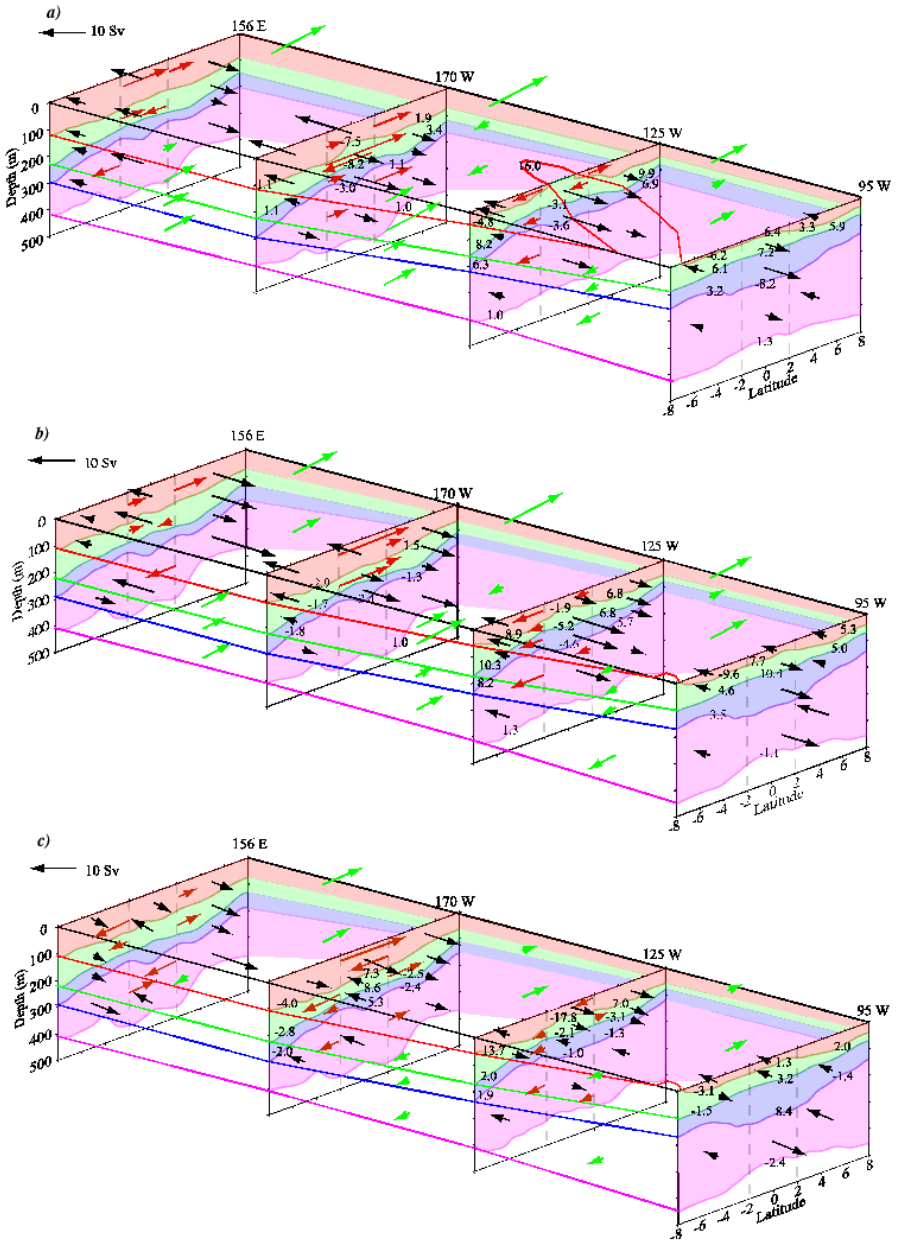

FIG. 7. Circulation ($\times 10^6$ m^3 s^{-1}) of the tropical Pacific for the 1990's composite El Niño at a) February +0, b) February +1 and c) the anomaly between February +1 and +0. The tropical Pacific Ocean is divided in 3 regions: western (western boundary-170°W); central (170°W-125°W); and eastern (125°W-eastern boundary). Ekman and geostrophic transports are combined in the meridional transport estimates. Lateral ($\pm 8^\circ$ green and $\pm 2^\circ$ red) and zonal (black) transports are indicated by solid arrows. Lateral transports at $\pm 2^\circ$ are shown on the western boundary of each region. Diapycnal transport between layer interfaces for southern, equator and northern sectors are shown on eastern boundary of each region. Only transports and anomalies greater than 1×10^6 m^3 s^{-1}are shown. Water classes are separated by bounding isopycnals surfaces – surface/mixed layer (red), upper thermocline (green), lower thermocline (blue), and thermostad (pink). Note that for the western Pacific, although the southern bound-

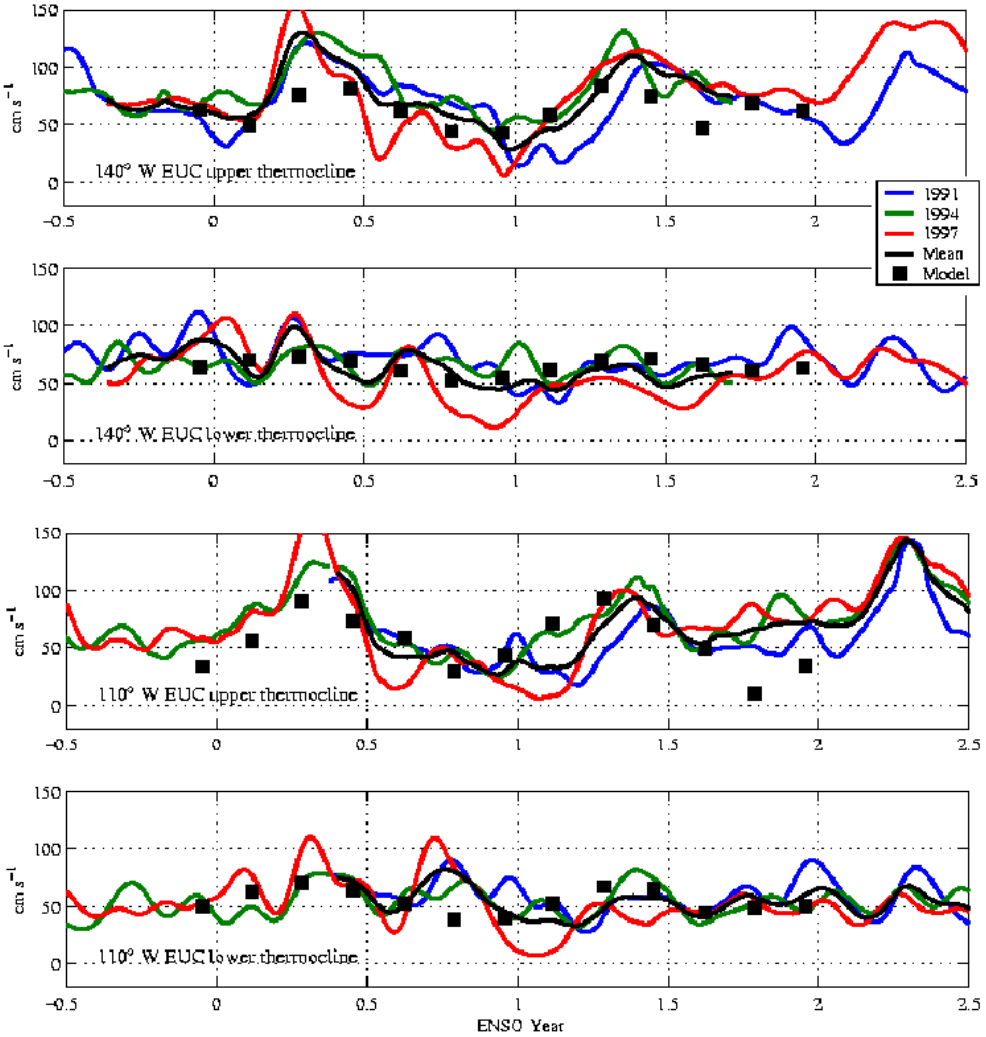

FIG. 8. EUC upper and lower thermocline vertically averaged velocities of the 60-day smoothed time-series ADCP zonal velocities from the TAO equatorial moorings at 140°W and 110°W for each individual El Niño event of the observation period of this study and their mean. The 13-bimonthly El Niño inverse model EUC upper and lower thermocline velocities (filled square) on the equator ($\pm 0.2°$) are also shown for the event cycle. Upper and lower thermocline water classes are as defined Table 1, and EUC as defined in Table 3.

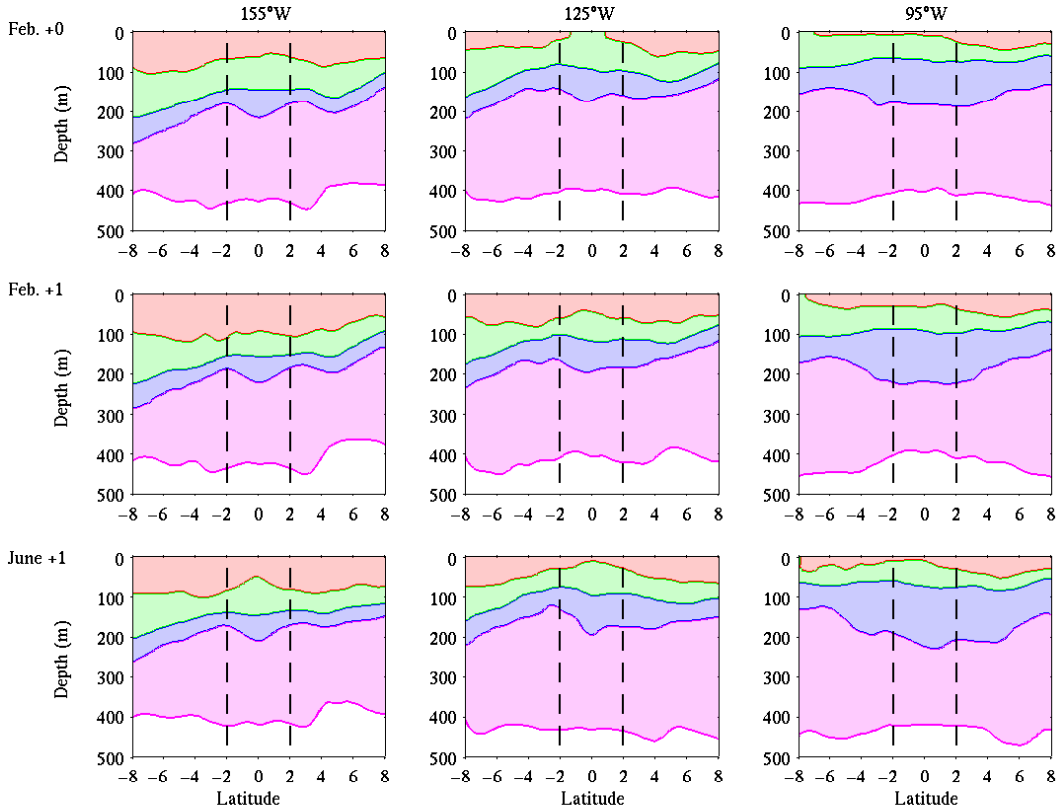

FIG. 9. Evolution of the thermocline structure in the central and eastern Pacific at 155°W, 125°W and 95°W from the onset (Feb. +0) to mature (Feb. +1) and decay (June +1) phases of the composite El Niño cycle. By June +1 the zonal thermocline slope has returned to normal. Subsequent Ekman upwelling in the central and eastern Pacific results in a sea-surface temperature cooling that signal the termination of El Niño. Water classes are as in Fig. 7.